Conformations and effective interactions of polymer coated nanoparticles at liquid interfaces

Konrad Schwenke,[†] Lucio Isa,[‡] David L. Cheung,[*,¶] and Emanuela Del Gado[*,†,§]

Department of Civil, Environmental and Geomatic Engineering, ETH Zürich, 8093 Zurich, Switzerland, Laboratory for Interfaces, Soft Matter and Assembly, Department of Materials, ETH Zürich, 8093 Zurich, Switzerland, Department of Pure and Applied Chemistry, University of Strathclyde, Glasgow G1 1XL, UK, and Department of Physics, Georgetown University, Washington, D.C. 20057, USA

E-mail: david.cheung@strath.ac.uk; delgado@ifb.baug.ethz.ch

Abstract

We investigate conformations and effective interactions of polymer-coated nanoparticles adsorbed at a model liquid-liquid interface via molecular dynamics simulations. The polymer shells strongly deform at the interface, with the shape governed by a balance between maximising the decrease in interfacial area between the two solvent components, minimising unfavourable contact between polymer and solvent and maximising the conformational entropy of the polymers. Using potential of mean force calculations we compute the effective interaction between the nanoparticles at the liquid-liquid interface. We find that it differs quantitatively from the bulk and is significantly affected by the length of the polymer chains and by the solvent quality.

[*]To whom correspondence should be addressed
[†]Department of Civil, Environmental and Geomatic Engineering, ETH Zürich
[‡]Department of Materials, ETH Zürich
[¶]Department of Pure and Applied Chemistry, University of Strathclyde
[§]Department of Physics, Georgetown University

Under good solvent conditions the effective interactions are always repulsive and soft for long chains. The repulsion range decreases as the solvent quality decreases. In particular, under poor solvent conditions, short chains may fail to induce steric repulsion, leading to a net attraction between the nanoparticles, whereas with long enough chains the effective interaction potential may feature an additional repulsive shoulder at intermediate distances.

Introduction

The self-assembly of nanoparticles (NPs) at liquid-liquid interfaces is a promising technology to create two-dimensional nano-structured materials.[1,2] In order to harness the potential for applications, it is necessary to control the particle-particle interactions at the interface. For instance, in the specific case of new materials with prescribed optical properties, e.g. in plasmonic sensing applications[3] or for the fabrication of liquid mirrors,[4] exact control over the distances between nanoparticles is crucial. Several specific interactions are present at liquid interfaces,[5] both attractive and repulsive, that can be controlled by tuning the nanoparticle surface properties. Unless necessary to produce highly elastic interfacial films, e.g. for food emulsion stabilization,[6] agglomeration of the particles, mostly due to attractive Van-der-Waals forces, is undesirable for maintaining interface fluidity and allowing the evolution of the interface microstructure towards equilibrium. Particle stabilization is often achieved via steric repulsion achieved by grafting polymers onto a solid nanoparticle core. The presence of the asymmetric environment, often implies that the requirements for stabilization at an interface are more stringent than in the bulk.[7] For instance, it has been shown that densely grafted poly(ethylene glycol) (PEG) brushes of molecular weight 1.5kDa provide excellent stabilization in bulk, even at high temperature, but fail to prevent aggregation at a water/n-decane interface.[8] Understanding the details of the interactions between polymer-stabilized nanoparticles at interfaces still presents many open questions and has direct practical relevance.

In most cases, NPs can be adsorbed at a liquid interface because the interfacial tension between the liquids is higher than between the NP and the liquids. Thus adsorption reduces the direct high energy contact area between the two solvents.[9] The effective adsorption energy for hard, spherical colloids has a simple geometrical dependence on radius and contact angle and can range from $\sim 10^6\ k_{\mathrm{B}}T$ for micron-sized particles[10] to 1-10 $k_{\mathrm{B}}T$ for nanometer sized particles.[11] Hence, the particles can be fairly irreversibly bound to the interface. A simple thermodynamic argument for the adsorption[9] predicts a parabolic shape for the interaction potential of a spherical particle with a flat interface; molecular simulations have shown that such simple thermodynamic arguments approximately hold for nanoparticles although microscopic effects such as capillary waves can become important.[12–14]

For polymer-coated nanoparticles the situation may be more complex. Polymers can also be adsorbed at the liquid interface, even in the absence of explicit amphiphilicity.[15] In the case of stabilizers with a length scale comparable to the NP size, the simple definitions of the contact line or of the particle size at the interface become non-trivial. The paradigm of spherical particles no longer necessarily holds and the full details of the interactions of the polymers with the two solvents and with the interface may be crucial in determining the adsorption energy. Measurements of the latter without any assumption on particle size and interface microstructure become therefore necessary.[16,17] In particular, recent measurements of PEG-grafted nanoparticles reported adsorption energies of the order of $1000k_{\mathrm{B}}T$,[17] indicating strong interfacial trapping. Recent simulations of dendrimers[18] have also shown that these can have adsorption energies comparable to nanoparticles; indeed in many cases the adsorption strength is higher for dendrimers due to their ability to change conformation at the interface to maximise the decrease in interfacial free energy and the interactions between the monomers and their preferred solvent. In the case of core-shell nanoparticles the polymer shell around the NP core may similarly deform at the interface, depending on the solvation quality of the liquids with regard to the polymers.[19–21] Conformations of polymer brushes at planar interfaces may switch between swollen chains for a good solvent to collapsed "dim-

ples" when the solvent quality decreases.[22] Small-angle neutron scattering experiments can provide insights into the density profiles of spherical polymer brushes[23] and light scattering can measure the hydrodynamic radius and hence the change in the shell thickness under different conditions,[24] but accessing directly the conformations of the polymer shells around the particles at a liquid interface is experimentally very challenging. Molecular simulations that can gain new insight into conformational changes and interactions at the atomistic level are extremely promising to complement the experiments. It has been indeed shown in numerical studies that hydrophobic chains at an air-water interface may display lense-shaped conformations.[19] For nanoparticles functionalized with short surfactants, numerical simulations have also indicated that the grafting density clearly affects their adsorption potential at an oil-water interface:[20] increasing the grafting density leads to enhanced adsorption energy as well as decreased shell deformability. With respect to the self-assembly of NPs within the interface, the effective interactions between NPs play an important role. For bare nanoparticles, attractive interactions due to the depletion of the solvent have been computed,[25–27] and recent works have also investigated forces between functionalized NPs in bulk water with explicit solvent.[28–30] Systematic investigations of the effective interactions of particles with a polymer shell have been successfully used for bulk systems in a supercritical solvent[31] or without explicit solvent,[32–36] but a translation of these findings to liquid interfaces is still lacking.

In this work, we aim at filling this gap and study conformations and effective interactions of polymer-coated NPs at liquid interfaces using numerical simulations with an explicit solvent model. We focus on the effect of the polymer conformations at the interface and of the solvent quality on the effective NP interactions. The paper is organised as follows: We first introduce our model, before we describe the main results for single particles at the interface, in particular the influence of the interface on the polymer conformations. Then, the effective interactions for two solvents which are identical in regard to the polymers are discussed and we present our results for the effective interactions in systems with a wetting

angle $\Theta_0 \neq 90°$. We close with a discussion of the results and concluding remarks.

Model and numerical details

We consider two immiscible liquids, with a diffuse interface between them, and core-shell nanoparticles which are adsorbed at the interface. The solvent particles are modelled as spheres interacting via a Lennard Jones potential

$$U(r) = 4\epsilon \left[(\sigma/r)^{12} - (\sigma/r)^{6}\right] \tag{1}$$

where σ is the particle diameter and r the inter-particle distance. The interaction is cut and shifted at a distance r_c so that $U(r_c) \cong 0$. In the following we will use the usual reduced units with ϵ as unit energy scale, σ as the unit length scale and all particles have unit mass m.

We consider two types of particles, A and B, to model the two liquids. The combination of repulsive interactions between A and B and attractive interactions between particles of the same type leads to the development of a stable interface between the two liquids. The Lennard-Jones potential is used for both types of interactions, but choosing $r_c = 2^{1/6}\sigma$ leaves only the repulsive part of the potential while $r_c = 2.5\sigma$ is used to model attractive interactions. This simple model is able to reproduce interfacial effects like capillary waves and nanoparticle adsorption and it has been successfully used to investigate effects at liquid-liquid interfaces with and without additional components.[14,18,37–39]

For a NP we use a large spherical particle as core onto which the first monomer of the polymer chains are grafted. The core and first monomers are treated as a rigid unit. We assume that, in absence of a strong anisotropy, the possibly irregular shape of the nanoparticle core can be neglected, especially when the polymer shell is dense enough that the chains are stretched and their length is on the order of, or larger than, the core size.[33] This description

translates into a shifted Lennard-Jones potential to model size differences between particles:

$$U(r) = 4\epsilon_{i,j}\epsilon\left[\left(\frac{\sigma}{r-\Delta}\right)^{12} - \left(\frac{\sigma}{r-\Delta}\right)^{6}\right], r < r_c + \Delta \tag{2}$$

where $\Delta = (\sigma_N - \sigma)/2$ and $\sigma_N = 8\sigma$ is the nanoparticle diameter. For $\Delta = 0$, Eq.(2) reduces to the usual Lennard-Jones potential. Bonded monomers interact via a harmonic potential $U = K(r - r_0)^2$ with $K = 125\epsilon/\sigma^2$ and $r_0 = 1\sigma$. All values of the parameters used for the interactions are given in table 1.

Changing the interaction strength $\epsilon_{a,b}$ between monomers and solvent allows us to tune the effective solvent quality with respect to the polymers. A value of $\epsilon_{a,b} = 1.0$ corresponds to good solvent conditions. Reducing $\epsilon_{a,b}$ changes the system towards the poor solvent case, and the polymers go from a swollen to a shrunk conformation. We will use $\epsilon_{a,b}$ when both solvents are identical with respect to the monomers and distinguish ϵ_a and ϵ_b otherwise.

We performed molecular dynamics simulations using the LAMMPS simulation package[40] in the NpT-ensemble, fixing the reduced temperature $k_{\mathrm{B}}T = 1.0\epsilon$ and the pressure $p = 1.0\epsilon\sigma^{-3}$. Temperature and pressure were controlled using Nosé-Hoover thermostat and barostat respectively,[41] with relaxation times of 0.5τ ($\tau = \sqrt{m\sigma^2/\epsilon}$ being the unit time). In order to localise the interface near the centre of the simulation box, repulsive walls were placed in the z-direction (with the z-axis normal to the interface and $z = 0$ marking the center of the simulation box). Periodic boundaries were applied in the x and y directions. If not stated otherwise, all data presented in the following are for particles with $N = 100$ chains grafted onto them and the number of monomers per chain $L = 5$ or 20. To simulate a system with two NPs, we used a cubic box of linear size $l_z = 100\sigma$ and $250 \cdot 10^3$ solvent molecules of each type, for the case in which the nanoparticles have chains made of $L = 20$ monomers. In the case of particles made with chains of $L = 5$ monomers, the box size is $l_z = 50\sigma$ and we used $28 \cdot 10^3$ solvent molecules of each type.

We have characterized the conformations of particles adsorbed at the liquid interface in

Table 1: Parameters used for the pair potentials.

Interaction	ϵ_{ij}	Δ	r_c
solvent: AA	1.0	0	2.5
solvent: AB	1.0	0	1.12246
core - core	1.0	7	1.12246
core - solvent	1.0	3.5	1.12246
core - monomer	1.0	3.5	1.12246
monomer - monomer	1.0	0	1.12246
monomer - solvent A	$\epsilon_a = 0.1$ - 1.0	0	2.5
monomer - solvent B	$\epsilon_b = 0.1$ - 1.0	0	2.5

the simulations of single nanoparticles in presence of the two solvents. From the simulations of pairs of NPs with the two solvents, we have computed the potential of mean force (PMF) and the distribution of solvent and monomers as a function of the distance R_{2d} between the particle cores in the interface plane. To sample different nanoparticle separations, the distance between the two particles has been constrained by a spring potential $U_{spring} = 0.5k_0(R_{2d} - R_0)^2$. For each set of parameters (chain number N, chain length L, solvent quality $\epsilon_{a,b}$), we chose a set of NP-distances R_0 such that the sampled nanoparticle distances R_{2d} overlap, and performed an independent simulation run for each R_0. For each set of values of the parameters we have equilibrated the related systems for 10^6 MD steps. The production runs took between 10^6 and $20 \cdot 10^6$ MD steps. The computation of the PMF as a function of the distance R_{2d} between the particle cores in the interface plane has been done using umbrella sampling.[14,42] The (biased) probability distribution $P_{R_0}(R_{2d})$ is determined from the data for runs with different R_0, and the final (unbiased) probability distribution $P(R_{2d})$ is determined using weighted histogram analysis.[43] The free energy is then given by $F(R_{2d}) = -k_{\mathrm{B}}T \ln[P(R_{2d})/R_{2d}]$.

Conformations of single particles at the interface and adsorption energies

For single particles at the liquid interface, the shape of the polymer shell is dictated by the competition between minimizing the monomer-solvent interface area, reducing the interface area between the two solvents and maximizing the conformational entropy of the polymers. Figure 1 displays the polymer density profiles computed by averaging over 150 conformations each separated by 10^4 MD steps. The density is binned in cylindrical coordinates, averaging over the angle φ since the polymers are grafted uniformly so that the system is symmetric with respect to rotations around the interface normal passing trough the NP center. The right and the left half of the disks in Fig. 1 are mirror images and were combined for the visual effect. The data show that, at the interface, the shells deviate from a spherical conformation, with the polymers forming a denser layer at the liquid interface and the chains at the interface being extended compared to the chains oriented towards the bulk. For particles in the poor solvent (Fig. 1 (a)) we find a compact polymer shell which is smoothly deformed towards the interface. Upon increasing the solvent quality, the polymer shell around the particle begins to swell (Fig. 1(b)) as the energy penalty associated with contact between the polymer and solvent becomes smaller. When the polymer is at the interface between two good solvents ($\epsilon_{a,b} = 1$) the minimisation of polymer-monomers surface area no longer matters and the polymers at the interface form a dense disk. There is a clear separation between polymers either being at the interface or pointing towards the bulk of the solvent (Fig. 1 (c)).

The influence of the liquid-liquid interface on the polymer conformation can be quantified by computing the average end-to-end distance of the chains R_e as a function of the angle α between the interface plane and the vector connecting their grafting point with the NP-center. The results plotted in Fig. 2 show the swelling of the chains with increasing solvent quality and the enhanced stretching of the chains closer to the interface. The data also indicate that the chains oriented toward the bulk are more stretched compared to free chains, an effect

that can be ascribed to the high grafting density of the polymer brush. The root mean square bond length in our model is $\sqrt{\langle b^2 \rangle} = 0.84\sigma$ and for a free self-avoiding chain[44] we would expect $R_e \simeq N^{0.588}\sqrt{\langle b^2 \rangle}$ so that $R_e(L = 5) \simeq 1.9\sigma$ and $R_e(L = 20) \simeq 4.7\sigma$, significantly smaller than what we see in Fig. 2.

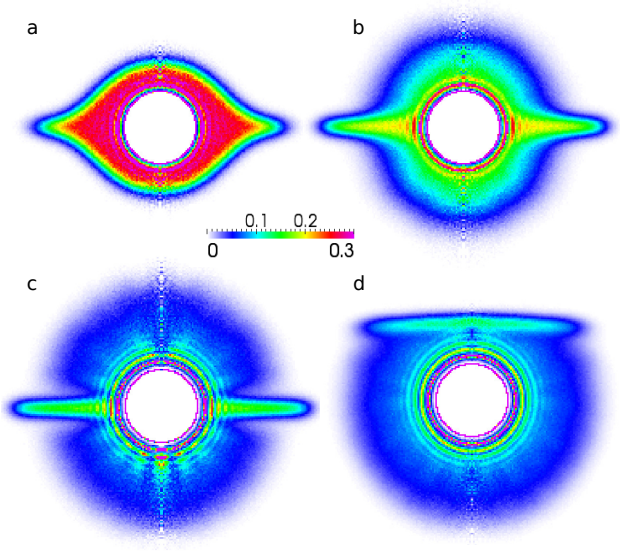

Figure 1: Density profiles of monomers around particles with polymer chain length $L = 20$ and monomer-solvent interaction strengths $\epsilon_a = \epsilon_b = 0.1$ (a), $\epsilon_a = \epsilon_b = 0.5$ (b), $\epsilon_a = \epsilon_b = 1.0$ (c), and $\epsilon_a = 1.0$ and $\epsilon_b = 0.7$ (d). The color code indicated by the bar in the middle gives the average number of beads per σ^3. The monomer density was binned in cylindrical coordinates, with the cylinder axis normal to the interface.

If the two solvents are of different quality, the particles will spend the majority of the time in the better solvent, and the overall shell conformation will be similar to the one in the better solvent, as can be seen in Fig. 1 (d). The particle core can be fully immersed in one phase, with only polymers being adsorbed at the interface, if the polymers are long enough compared to the core size. In our model, we indeed observe this for $L = 20$ but not for $L = 5$. Our findings are consistent with the results of numerical simulations of gold nanoparticles grafted with hydrophobic polymers at the air-water interface in Ref. 19. In particular, we notice a similarity between the density profiles obtained in Ref. 19 and the ones we find for the poor solvent case (Fig. 1 a)). Polymer orientation towards the liquid

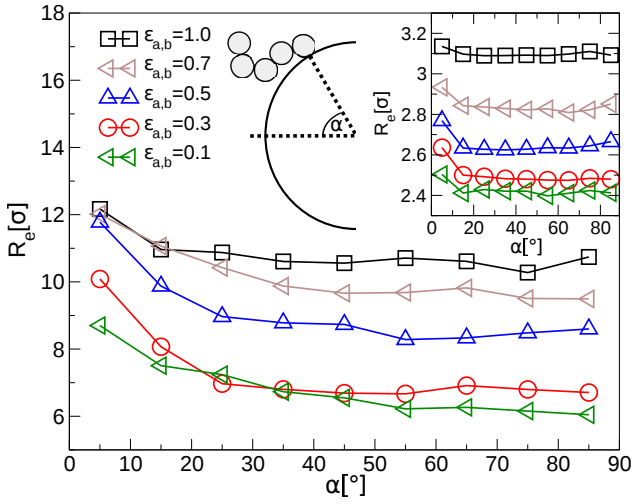

Figure 2: End-to-end distance R_e of the grafted polymers as a function of the angle α between the interface plane and the vector connecting their grafting point with the NP-center (see the cartoon in the center) for particles with $L = 20$. Small angles correspond to chains close to the interface. Inset: The same for $L = 5$.

interface has been reported in the simulations of polymer-covered nanoparticles in Ref. 20, although the polymer chains considered there are relatively short with respect to the linear size of the solvent molecules.

Finally, for different combinations of monomer-solvent interactions, we have computed the contour plot of the equilibrium distance $\langle |z| \rangle$ of NPs from the interface. In Fig. 3 the data for $L = 20$ are shown; not only the polymer conformation but also the exact particle position depends on the combination of solvents. The larger the discrepancy, the further away from the interface the particle resides. When the distance from the interface becomes greater than the core radius, this indicates that only the polymer shell is in contact with the interface. With decreasing solvent quality, nevertheless, the difference between ϵ_a and ϵ_b becomes less important.

From the equilibrated conformation of a NP at the interface in the different conditions just described, we can also get an estimate for the desorption energies of the NPs. This has been done by switching on a spring force which acts on the core-particle of the NP and pulls it towards a position z_0 in the bulk. The energy stored in the spring is $E =$

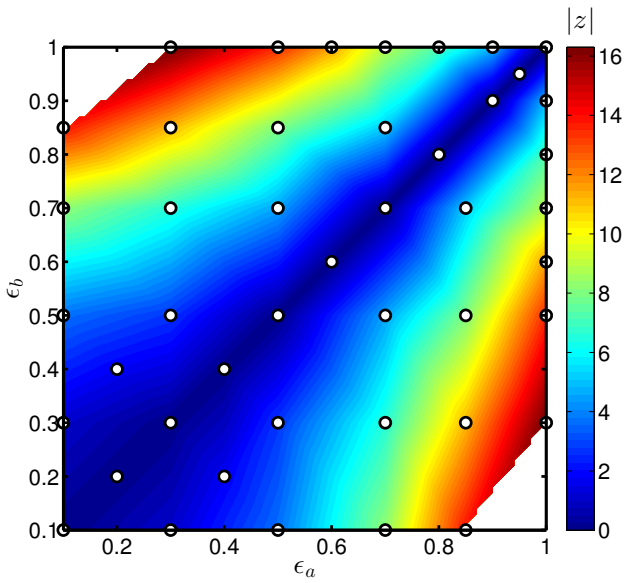

Figure 3: Contour plot of the equilibrium distance $\langle|z|\rangle$ from the interface for the NPs with $L = 20$ at different combinations of monomer-solvent interaction strength ϵ_a and ϵ_b. The white dots mark the values which were used for the interpolation.

$0.5k(z_{\text{equilibrium}} - z_0)^2$. By varying the spring constant k we can get a rough estimate of the energy needed to detach the particle from the interface. Specifically this gives an upper limit for the desorption energy ΔE. The results in Table 2 indicate again that adsorption of the particles at the interface is essentially irreversible with $\Delta E \gg k_{\text{B}}T$. Moreover we find a decrease in ΔE with decreasing solvent quality and with decreasing chain length as theoretically expected.[45] The limits of this approach beyond a qualitative comparison are shown by $\Delta E = 350k_{\text{B}}T$ for the bare NP. With an interfacial tension of $\gamma = 1.55\epsilon\sigma^{-2}$ in our model, the expected adsorption energy for a bare particle of diameter 8σ would only be $80k_{\text{B}}T$.[9] Nevertheless, the fact that the values for the NPs with $L = 20$ are of the same order of magnitude as found experimentally for NPs with a PEG-shell[17] supports the choice of our model parameters.

Table 2: Estimates for the upper limits of the NP desorption energies for particles with $N = 100$ and without a polymer shell.

$\epsilon_{a,b}$	$L = 20$	$L = 5$
1.0	$4500k_{\mathrm{B}}T$	$850k_{\mathrm{B}}T$
0.5	$2000k_{\mathrm{B}}T$	$750k_{\mathrm{B}}T$
0.1	$1800k_{\mathrm{B}}T$	$700k_{\mathrm{B}}T$
bare particle	$350k_{\mathrm{B}}T$	

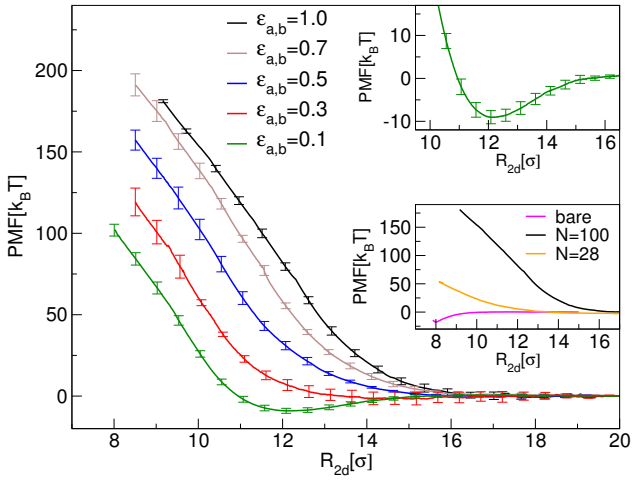

Figure 4: Potential of mean force for the interaction of two NPs at the interface with $N = 100$ monomers in each polymer chain and chain length $L = 5$ with different strengths $\epsilon_{a,b}$ for the monomer-solvent interaction. For the interface systems, R_{2d} is the distance in the 2d-interface plane. Top Inset: Detail of the PMF with $\epsilon_a = \epsilon_b = 0.1$ and $N = 100$. Bottom Inset: PMF for a bare NP without polymer shell and NPs with $\epsilon_a = \epsilon_b = 1$ and $N = 100$ and $N = 28$ chains grafted onto them.

Effective NP-interactions for equal solvent qualities

We consider two NPs at the interface connected by a spring force holding them within a given distance of each other and calculate the effective interaction potential between them via umbrella sampling. The time series from the simulations is divided in 4 equal parts and each part is analyzed independently to obtain a potential of mean force (PMF). The time series data are then averaged and the sample-to-sample fluctuations used to obtain the error bars. The interaction potential is computed as a function of the 2-dimensional distance R_{2d} between the particle cores in the interface plane.

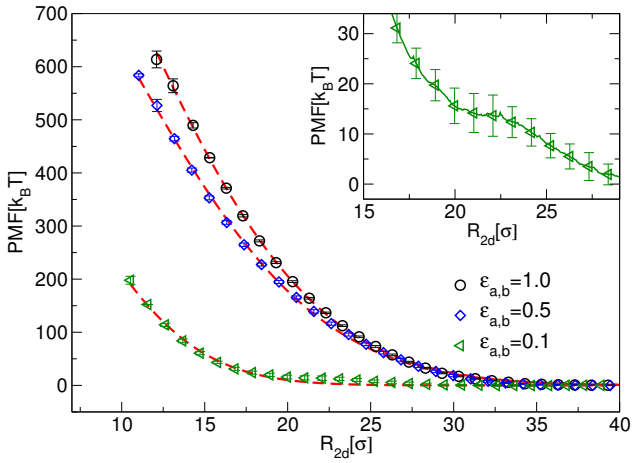

Figure 5: Potential of mean force for the interaction of two NPs at the interface with chain length $L = 20$ and different strength $\epsilon_{a,b}$ for the monomer-solvent interaction. The red lines are fits with the Gaussian potential $U(R) = \epsilon_g \exp(-(R/\sigma_g)^2)$. Inset: Detail of the PMF with $\epsilon_a = \epsilon_b = 0.1$.

Figure 4 displays the PMF as a function of the interparticle distance at the interface for $L = 5$ and for different strengths of the solvent-solvent interactions. In all cases discussed here we consider the same polymer solvation for the two solvents. The bare NPs, whose linear size is only a factor 8 larger than the solvent particles, experience an effective attraction due to depletion effects (top inset in Fig. 4). This result is consistent with the findings of other molecular simulations.[25,27] Nevertheless we find that a polymer shell of short chains can screen the attractive interactions and induce a net steric repulsion. The pronounced differences in the shape of the polymer shell in Fig. 1 suggest that the effective interactions between the core-shell particles at the interface depend on the solvent quality. Indeed, we find that the range of the repulsive interaction is strongly affected by the swelling of the polymers. Finally the grafting density of the polymer brush also influences the range of the effective potential substantially via the effect on the chain conformations, as shown in the inset of Fig. 4, where the PMFs of particles with two different grafting densities are compared.

Similar features are present in the PMF for $L = 20$ for different solvent qualities, as shown in Fig. 5. In addition, the figure shows that the PMF can be well fitted over the

whole range by a Gaussian potential $U(r) = \epsilon_g \exp(-(r/\sigma_g)^2)$ (dashed lines), as predicted by Flory's theory for dilute polymer solutions.[46] Such finding is in good agreement with previous numerical results for interacting spherical polymer brushes.[32,35] Despite the fact that the theory should describe only interactions between the outer regions of the polymer shell, we see that the Gaussian function fits the whole range of particle distances within the precision of our calculation. We also notice that the Gaussian fit does not work for the short chains of Fig. 4, most probably due to the cores whose linear size, in that case, is much larger than the polymer chain length: Fig. 4 shows that for chain length $L = 5$ the net effective interactions are more dominated by the cores, with a power law type of repulsive potential. The influence of the core at close distances[35] is probably also the reason why we do not detect, at short distances, the logarithmic dependence typical of the interactions between two spherical polymer brushes.[32,47] Finally we notice that, for long chains ($L = 20$) with the poor solvents, the effective interaction potential displays a shoulder as shown in the inset of Fig. 5. This feature in the effective interaction could favor the formation of stripes or dimer patterns in the NPs assembly at the liquid interface.[48–50]

We investigate the change in the chain conformations corresponding to different inter-NP distances, by calculating the average end-to-end distance of the chains as a function of the NP distance R_{2d}. Since we are interested in the chains at the interface, residing between the NPs, we consider only polymers whose grafting point lies in the volume between the NP-cores. The results, plotted in Fig. 6, show that chains at the interface are at first compressed upon approach (roughly $12\sigma \lesssim R_{2d} \lesssim 16\sigma$ for $L = 5$ and $18\sigma \lesssim R_{2d} \lesssim 30\sigma$ for $L = 20$, respectively). Upon closer contact, the chains are stretched again when they are squeezed out from the volume between the NPs. The first compression is more pronounced due to the fact that chains are originally swollen at the interface, but this effect can also be observed in bulk systems[35,51].[52]

In Fig. 7 we plot the average distance of the particle from the interface as a function of the NP distance R_{2d} for $L = 20$: the data show that pushing the NPs together over distances

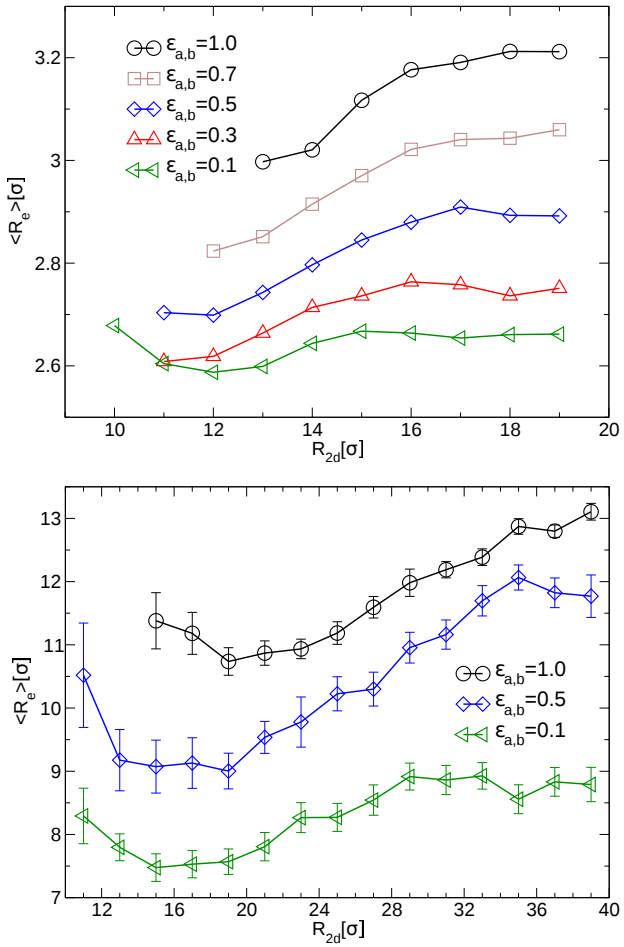

Figure 6: End-to-end distance of the polymers whose first monomer lies in the toroid volume between the two NPs and within $\pm 1\sigma$ in z-direction from the NP-center, as function of the NP-distance R_{2d} for different strengths $\epsilon_{a,b}$ of the monomer-solvent interaction for $L = 5$ (top) and $L = 20$ (bottom).

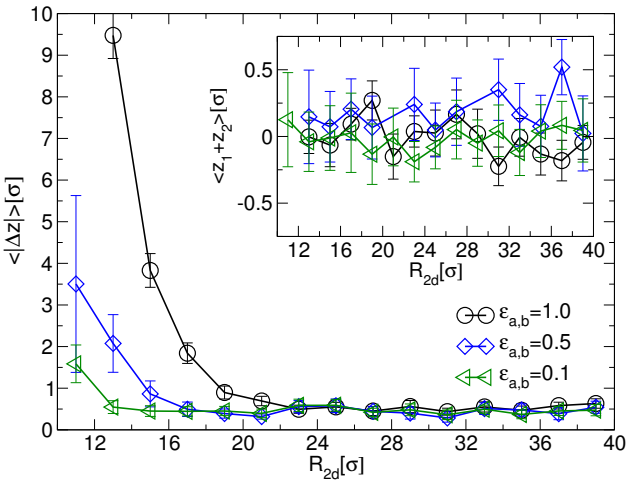

Figure 7: Mean height difference between the two NPs with $L = 20$ as a function of their distance R_{2d}. Inset: Asymmetricity of particle detachment from the bulk measured by $z_1 + z_2$ where z_1 and z_2 are the z-coordinate of the core of NP 1 and NP 2, respectively.

even shorter than the one explored in Fig. 6 moves them eventually away from the interface plane and partially detaches them from the interface. Since both solvents interact in the same way with the NPs, the particles are displaced symmetrically (see inset of Fig. 7).

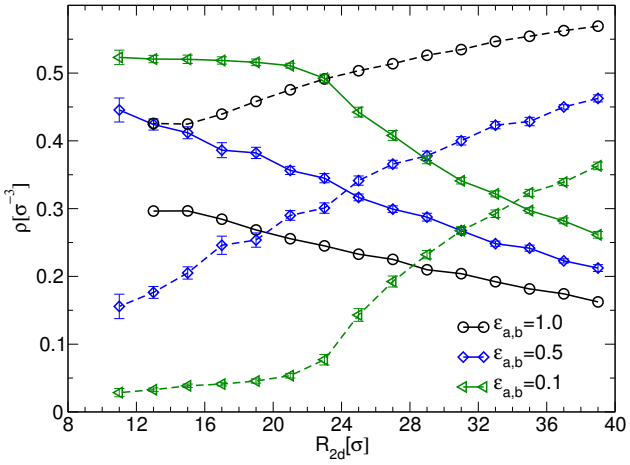

Figure 8: Concentration of monomers (bold lines) and solvent particles (dashed lines) between the two NPs as function of the NP-distance R_{2d} for different strengths $\epsilon_{a,b}$ of the monomer-solvent interaction.

In order to unravel the physical mechanisms at the origin of the qualitative differences in the PMF, we have first monitored the concentrations ρ_s and ρ_m of, respectively, solvent

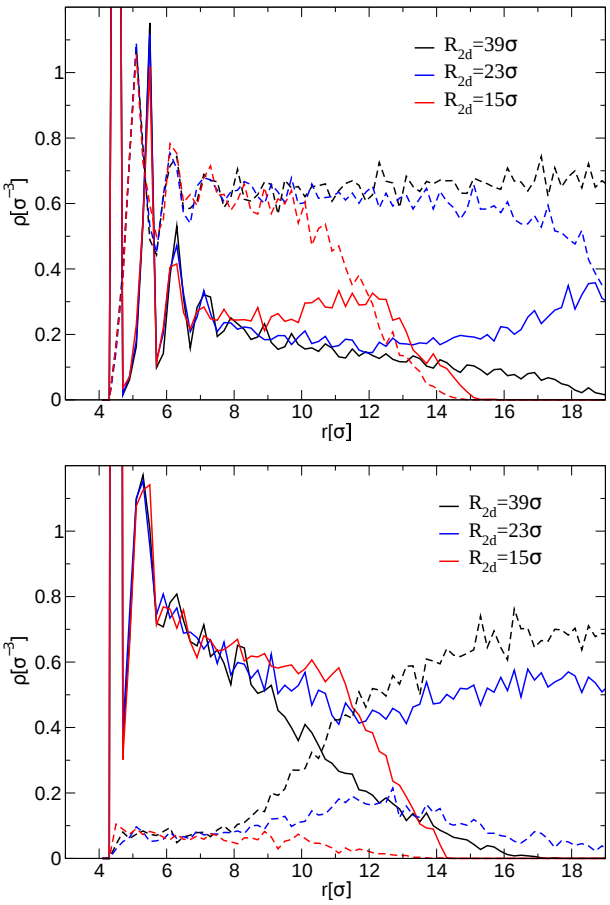

Figure 9: Radial density profiles of monomers (bold lines) and solvent (dashed lines) around the nanoparticle core, considering only monomers / solvent particles which are in the volume between the two NPs for $\epsilon_a = \epsilon_b = 1.0$ (top) and $\epsilon_a = \epsilon_b = 0.1$ (bottom) for systems with $L = 20$.

molecules and monomers between the NPs as a function of their distance R_{2d}. The results are plotted in Fig. 8 for different solvent qualities. The data show that the solvent initially filling the gap between the NPs is progressively expelled upon their approach. For $\epsilon_a = 1$, the solvent penetrates the polymer shell and $\rho_s \geq \rho_m$ for the whole range of R_{2d} for which the NPs do not detach from the interface, as there is no preference for a monomer to be surrounded by solvent molecules or by other monomers. Upon decreasing R_{2d}, we observe a relative increase of ρ_m with respect to ρ_s, indicating that the solvent is expelled from the region between the two NPs. At even smaller inter-particle distances, the data show that both the polymer chains and the solvent molecules are squeezed out, away from the interface.

For decreasing solvent quality, the data in Fig. 8 also show that solvent and monomers tend to segregate, so that for $\epsilon_{a,b} = 0.1$ hardly any solvent is left between NPs at close distances. To elucidate this point further, we compute the density profile of solvent and monomers in the volume between the NPs, shown in Fig. 9. Overall, close enough to the NP-core, the solvent density is essentially independent of R_{2d}. Nevertheless, whereas in the good solvent case the polymers are swollen, in the poor solvent case the polymers are in a *melt* state, with hardly any solvent left. As a consequence, in the poorest solvent investigated, the polymer shell compactifies so strongly, that for the NPs with short polymers ($L = 5$) interactions are similar to the ones between bare cores, only with a larger effective diameter given by the core and shell size (see the inset of Fig. 4 and Fig. 6).

By comparing the different regimes in the PMF with the concentration of solvent molecules between the NPs in Fig. 8 we gain some further understanding. At large distances, being unfavourable to expel solvent molecules from the low density interface region into the bulk,[53] the PMF is essentially determined by the effective interaction in the polymer melt, which cancels out the attractive depletion interaction between cores. Hence at short distances, where the strength of the repulsion is around $15k_{\mathrm{B}}T$, the chains at the interface are fairly compressed (see Fig. 6). At even shorter distances, the chains are squeezed out from the volume between the NPs and core-core interactions dominate, with the PMF increasing to

more than $100k_{\mathrm{B}}T$.

Polymers with different solvent affinities

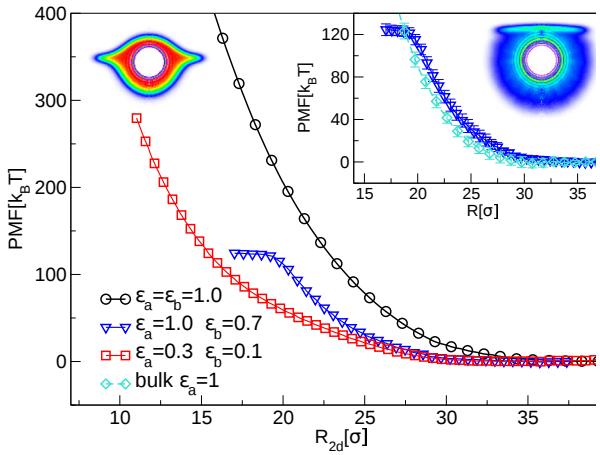

Figure 10: Potential of mean force for the interaction of two NPs at the interface with chain length $L = 20$ and different strengths ϵ_a and ϵ_b for the monomer-solvent interaction. Inset: Comparison of interaction in the bulk with $\epsilon_a = 1$ and for the system with $\epsilon_a = 1$ and $\epsilon_b = 0.7$.
The images of the mean monomer densities are for $\epsilon_a = 0.3$, $\epsilon_b = 0.1$ (top left) and $\epsilon_a = 1.0$, $\epsilon_b = 0.7$ (top right). The color code is the same as in Fig. 1.

In most experimentally relevant situations, the two liquids forming the interface will interact differently with the polymer shell of the NPs. When the interaction strengths ϵ_a and ϵ_b differ for the two solvents, the NPs may still be adsorbed, but the majority of the particle will reside in the better solvent (see Fig. 3). In Fig. 10 we plot the PMF computed with solvent of different qualities: the data show that upon increasing the solvation disparity between the two solvents ($\epsilon_a = 1.0$ and $\epsilon_b = 0.7$), the PMF can develop a kink around $120k_{\mathrm{B}}T$, where one of the two particles is desorbed and pushed into the bulk phase. Fig. 11 displays indeed the corresponding mean height difference between NPs indicating that, differently from the symmetric solvent case, for large solvation disparities only one of the particles detaches from the interface whereas the other one remains at the equilibrium position. The findings for this particular asymmetric enough good solvent case can be rationalised by considering that

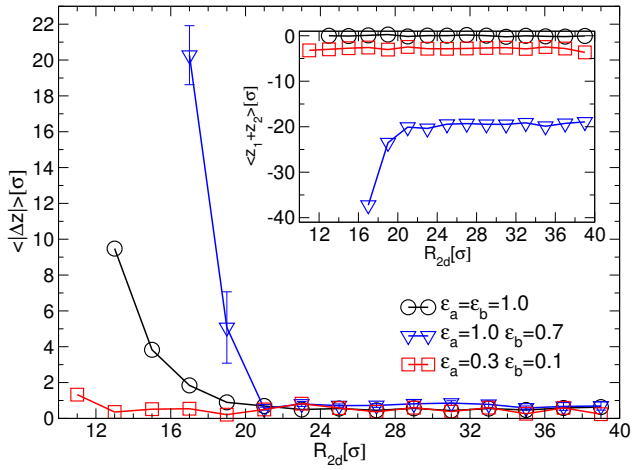

Figure 11: Mean height difference between NPs with different strengths ϵ_a and ϵ_b for the monomer-solvent interaction as a function of their distance R_{2d}. Inset: Asymmetricity of particle detachment from the bulk measured by $z_1 + z_2$ where z_1 and z_2 are the z-coordinate of the core of NP 1 and NP 2, respectively.

the particles interact first through chains in the bulk. Because the NPs are submerged, the chains adsorbed at the interface won't have the same extension as in the symmetric case (see Fig. 1). Therefore, the range of the NP interaction is lower compared to the symmetric case and the PMF is more similar to the interaction of NPs in the bulk, until one of the NPs eventually desorbs (Inset of Fig. 11). The picture changes for a combination of poor solvents ($\epsilon_a = 0.3$ and $\epsilon_b = 0.1$): also there the majority of the particle resides in the better solvent, but it remains closer to the interface and the chains at the interface are more extended than in the bulk. Hence, the behavior upon approach is more similar to the symmetric solvent systems, including the fact that the particles displace symmmetrically with respect to their equilibrium position upon decreasing R_{2d} (Inset of Fig. 11). In general, we expect that length, grafting density and surface activity of the polymer, in addition to the two solvent qualities, influence the interaction mechanism between the nanoparticles.

Conclusion

From simulations of isolated nanoparticles it can be seen that the polymer shell around the particle undergoes significant deformation at the interface. Overall the particle shell adopts a lense shape, with the chains expanding in the plane of the interface, which reduces the interfacial area between the two solvent components, decreasing the interfacial free energy, or the unfavourable polymer-solvent interfaces in the case of poor solvents. Increasing the solvent quality decreases the asphericity, due to the polymer chains swelling. When the polymer has a sufficiently distinct affinity for one of the solvent components, the particle can move away from the interface, although a region of high polymer concentration remains in the vicinity of the interface, acting as a surfactant to reduce the interfacial free energy. Hence changing the solvent affinity also provides a straight forward route to control the effective contact angle of the particle. We have also estimated the adsorption energy from the energy needed to remove a particle from the interface once it is adsorbed. The results are consistent with the high adsorption energy values measured in experiments on polymer shell nanoparticles.[17,54]

Using potential of mean force calculations, we found that in the absence of any polymer chains the NP effective interaction is attractive.[55] The polymer shell screens the attraction and the net interaction is repulsive, in a similar manner to sterically stabilised nanoparticles in bulk solution. The strength and range of this repulsion depends on the solvent quality; for nanoparticles at the interface between good solvents the range and strength increases because the polymer chains swell. Increasing the chain length of the polymer shell increases the interaction range. For long chains in poor solvent two distinct length scales may characterise the effective interactions, because a well defined separation may emerge between a solvent-poor region between the particles at intermediate distances and the region of high polymer density at much shorter distances, a type of interaction which might favour stripe patterns at the interface.[56] Pushing together the particles causes the particles to detach from the interface, suggesting that at short ranges the repulsion strength becomes comparable to

the interfacial adsorption strength for the nanoparticles. When the interaction between the polymer chains and the solvents are the same for both components the change in position relative to the interface is roughly symmetrical. For large solvation disparity, instead, one particle is repelled into the bulk while the other remains in the vicinity of the interface.

As liquid-liquid interfaces are potentially convenient and elegant templates for the formation of nanoparticle structures, understanding the interactions between particles in these environments is a key step in material optimisation. Changing the lengths of attached polymer chains provides a chemically straightforward route to changing the interactions between particles and hence controlling the structure formation, as it has been already observed in experiments.[45,57] Further work will involve investigations of the effect of polymer density and architecture on the interactions between nanoparticles at liquid interfaces and the use of the effective potentials determined in this work for numerical studies of nanoparticle self-assembly.

Acknowledgement

KS and EDG were supported by the Swiss National Science Foundation (Grant No. PP00P2_126483/1 and PP00P2_150738) and LI was supported by the SNSF grants PZ00P2_142532/1 and PP00P2_144646/1. DLC was supported in the initial stages of this work by the Leverhulme Trust (ECF/2010/0254).

Supporting Information Available

PMF for particles in the bulk with and without explicit solvent. End-to-end distance of the polymers between the particles in the bulk. Additional simulation data for particles with $L = 5$: Solvent and monomer concentration between particles as function of R_{2d}. Mean height differences between particles as function of R_{2d}. This material is available free of charge via the Internet at `http://pubs.acs.org/`.

Notes and References

(1) Popp, N.; Kutuzov, S.; Böker, A. Various Aspects of the Interfacial Self-Assembly of Nanoparticles. Adv. Poly. Sci. **2010**, 228, 39–58.

(2) Grzelczak, M.; Vermant, J.; Furst, E. M.; Liz-Marzán, L. M. Directed self-assembly of nanoparticles. ACS Nano **2010**, 4, 3591–605.

(3) Turek, V. A.; Cecchini, M. P.; Paget, J.; Kucernak, A. R.; Kornyshev, A. A.; Edel, J. B. Plasmonic ruler at the liquid-liquid interface. ACS Nano **2012**, 6, 7789–99.

(4) Fang, P.-P.; Chen, S.; Deng, H.; Scanlon, M. D.; Gumy, F.; Lee, H. J.; Momotenko, D.; Amstutz, V.; Cortés-Salazar, F.; Pereira, C. M.; Yang, Z.; Girault, H. H. Conductive gold nanoparticle mirrors at liquid/liquid interfaces. ACS Nano **2013**, 7, 9241–8.

(5) Bresme, F.; Oettel, M. Nanoparticles at fluid interfaces. J. Phys. Condens. Matter **2007**, 19, 413101.

(6) Dickinson, E. Proteins at interfaces and in emulsions Stability, rheology and interactions. J. Chem. Soc. Faraday Trans. **1998**, 94, 1657–1669.

(7) Garbin, V.; Crocker, J. C.; Stebe, K. J. Nanoparticles at fluid interfaces: Exploiting capping ligands to control adsorption, stability and dynamics. J. Colloid Interface Sci. **2012**, 387, 1–11.

(8) Isa, L.; Amstad, E.; Textor, M.; Reimhult, E. Self-Assembly of Iron Oxide-Poly(ethylene glycol) CoreShell Nanoparticles at LiquidLiquid Interfaces. Chim. Int. J. Chem. **2010**, 64, 145–149.

(9) Pieranski, P. Two-dimensional interfacial colloidal crystals. Phys. Rev. Lett. **1980**, 45, 569–572.

(10) Binks, B. P. Particles as surfactants: similarities and differences. Curr. Opin. Coll. Inter. Sci. **2002**, 7, 21–41.

(11) Du, K.; Glogowski, E.; Emrick, T.; Russell, T. P.; Dinsmore, A. D. Adsorption Energy of Nano- and Microparticles at Liquid-Liquid Interfaces. Langmuir **2010**, 26, 12518–12522.

(12) Bresme, F.; Quirke, N. Nanoparticulates at liquid/liquid interfaces. Phys. Chem. Chem. Phys. **1999**, 1, 2149–2155.

(13) Cheung, D.; Bon, S. Interaction of Nanoparticles with Ideal Liquid-Liquid Interfaces. Phys. Rev. Lett. **2009**, 102, 13–16.

(14) Cheung, D. L. Molecular dynamics study of nanoparticle stability at liquid interfaces: Effect of nanoparticle-solvent interaction and capillary waves. J. Chem. Phys. **2011**, 135, 054704–054712.

(15) Halperin, A.; Pincus, P. Polymers at a liquid-liquid interface. Macromolecules **1986**, 19, 79–84.

(16) Garbin, V.; Crocker, J. C.; Stebe, K. J. Forced desorption of nanoparticles from an oil-water interface. Langmuir **2012**, 28, 1663–7.

(17) Zell, Z. A.; Isa, L.; Ilg, P.; Leal, L. G.; Squires, T. M. Adsorption Energies of Poly(ethylene oxide)-Based Surfactants and Nanoparticles on an Air-Water Surface. Langmuir **2014**, 30, 110–9.

(18) Cheung, D. L.; Carbone, P. How stable are amphiphilic dendrimers at the liquidliquid interface? Soft Matter **2013**, 6841–6850.

(19) Tay, K.; Bresme, F. Wetting properties of passivated metal nanocrystals at liquid-vapor interfaces: a computer simulation study. J. Am. Chem. Soc. **2006**, 128, 14166–14175.

(20) Ranatunga, R. J. K. U.; Kalescky, R. J. B.; Chiu, C.-c.; Nielsen, S. O. Molecular Dynamics Simulations of Surfactant Functionalized Nanoparticles in the Vicinity of an Oil/Water Interface. J. Phys. Chem. C **2010**, 114, 12151–12157.

(21) Lane, J. M. D.; Grest, G. S. Spontaneous Asymmetry of Coated Spherical Nanoparticles in Solution and at Liquid-Vapor Interfaces. Phys. Rev. Lett. **2010**, 104, 235501.

(22) Dimitrov, D. I.; Milchev, A.; Binder, K. Polymer brushes in solvents of variable quality: molecular dynamics simulations using explicit solvent. J. Chem. Phys. **2007**, 127, 084905.

(23) Förster, S.; Wenz, E.; Lindner, P. Density Profile of Spherical Polymer Brushes. Phys. Rev. Lett. **1996**, 77, 95–98.

(24) Shortell, M. P.; Fernando, J. F. S.; Jaatinen, E. a.; Waclawik, E. R. Accurate measurement of the molecular thickness of thin organic shells on small inorganic cores using dynamic light scattering. Langmuir **2014**, 30, 470–6.

(25) Powell, C.; Fenwick, N.; Bresme, F.; Quirke, N. Wetting of nanoparticles and nanoparticle arrays. Colloids Surfaces A Physicochem. Eng. Asp. **2002**, 206, 241–251.

(26) Ranatunga, R. J. K. U.; Nguyen, C. T.; Wilson, B. a.; Shinoda, W.; Nielsen, S. O. Molecular dynamics study of nanoparticles and non-ionic surfactant at an oilwater interface. Soft Matter **2011**, 6942–6952.

(27) Fan, H.; Striolo, A. Nanoparticle effects on the water-oil interfacial tension. Phys. Rev. E **2012**, 86, 051610–051621.

(28) Jenkins, S.; Kirk, S. R.; Persson, M.; Carlen, J.; Abbas, Z. Molecular dynamics simulation of nanocolloidal amorphous silica particles: Part I. J. Chem. Phys. **2007**, 127, 224711.

(29) Lane, J.; Ismail, A.; Chandross, M.; Lorenz, C.; Grest, G. Forces between functionalized silica nanoparticles in solution. Phys. Rev. E **2009**, 79, 050501.

(30) Salerno, K. M.; Ismail, A. E.; Lane, J. M. D.; Grest, G. S. Coating thickness and

coverage effects on the forces between silica nanoparticles in water. J. Chem. Phys. **2014**, 140, 194904.

(31) Sun, L.; Yang, X.; Wu, B.; Tang, L. Molecular simulation of interaction between passivated gold nanoparticles in supercritical CO2. J. Chem. Phys. **2011**, 135, 204703.

(32) Cerdà, J. J.; Sintes, T.; Toral, R. Pair Interaction between End-Grafted Polymers onto Spherical Surfaces: A Monte Carlo Study. Macromolecules **2003**, 36, 1407–1413.

(33) Tay, K.; Bresme, F. Computer simulations of two dimensional gold nanoparticle arrays: the influence of core geometry. Mol. Simul. **2005**, 31, 515–526.

(34) Schapotschnikow, P.; Vlugt, T. J. H. Understanding interactions between capped nanocrystals: three-body and chain packing effects. J. Chem. Phys. **2009**, 131, 124705.

(35) Lo Verso, F.; Yelash, L.; Egorov, S. a.; Binder, K. Interactions between polymer brush-coated spherical nanoparticles: the good solvent case. J. Chem. Phys. **2011**, 135, 214902.

(36) Lo Verso, F.; Egorov, S. A.; Binder, K. Interaction Between Polymer Brush-Coated Spherical Nanoparticles: Effect of Solvent Quality. Macromolecules **2012**, 45, 8892–8902.

(37) Stecki, J.; Toxvaerd, S. The liquid liquid interface of simple liquids. J. Chem. Phys. **1995**, 103, 4352.

(38) Diaz-Herrera, E.; Alejandre, J.; Ramirez-Santiago, G.; Forstmann, F. Interfacial tension behavior of binary and ternary mixtures of partially miscible Lennard-Jones fluids: A molecular dynamics simulation. J. Chem. Phys. **1999**, 110, 8084.

(39) Simmons, V.; Hubbard, J. B. Molecular dynamics study of the surface tension of a binary immiscible fluid. J. Chem. Phys. **2004**, 120, 2893–900.

(40) Plimpton, S. Fast parallel algorithms for short-range molecular dynamics. J. Comput. Phys. **1995**, 117, 1–19.

(41) Martyna, G.; Tobias, D.; Klein, M. L. Constant pressure molecular dynamics algorithms. J. Chem. Phys. **1994**, 101, 4177.

(42) Torrie, G.; Valleau, J. Nonphysical sampling distributions in Monte Carlo free-energy estimation: Umbrella sampling. J. Comput. Phys. **1977**, 23, 187–199.

(43) Kumar, S.; Rosenberg, J. M.; Bouzida, D.; Swendsen, R. H.; Kollman, P. A. The weighted histogram analysis method for free-energy calculations on biomolecules. I. The method. J. Comput. Chem. **1992**, 13, 1011–1021.

(44) Rubinstein, M.; Colby, R. H. Polymer Physics; Oxford University Press, 2003.

(45) Isa, L.; Amstad, E.; Schwenke, K.; Del Gado, E.; Ilg, P.; Kröger, M.; Reimhult, E. Adsorption of core-shell nanoparticles at liquid liquid interfaces. Soft Matter **2011**, 7, 7663–7675.

(46) Flory, P. J. Principles of polymer chemistry; Cornell University Press: Ithaca, 1978; p 672.

(47) Witten, T.; Pincus, P. Colloid stabilization by long grafted polymers. Macromolecules **1986**, 19, 2509–2513.

(48) Malescio, G.; Pellicane, G. Stripe phases from isotropic repulsive interactions. Nat. Mater. **2003**, 2, 97–100.

(49) Imperio, A.; Reatto, L. A bidimensional fluid system with competing interactions: spontaneous and induced pattern formation. J. Phys. Condens. Matter **2004**, 16, S3769–S3789.

(50) Camp, P. J. Structure and dynamics in a monolayer of core-softened particles. J. Mol. Liq. **2006**, 127, 10–13.

(51) See supplemental material for further information.

(52) In Ref. 35, the radius of gyration of all chains was calculated as a function of NP-separation and so this effect could be easily overlooked, especially compared to the significant stretching of chains when they are squeezed out from the volume between the NPs.

(53) Carson Meredith, J.; Sanchez, I. C.; Johnston, K. P.; de Pablo, J. J. Simulation of structure and interaction forces for surfaces coated with grafted chains in a compressible solvent. J. Chem. Phys. **1998**, 109, 6424.

(54) Schwenke, K.; Isa, L.; Del Gado, E. Assembly of nanoparticles at liquid interfaces: crowding and ordering. Langmuir **2014**, 30, 3069–74.

(55) Bresme, F.; Lehle, H.; Oettel, M. Solvent-mediated interactions between nanoparticles at fluid interfaces. J. Chem. Phys. **2009**, 130, 214711.

(56) Sear, R. P.; Chung, S.-W.; Markovich, G.; Gelbart, W. M.; Heath, J. R. Spontaneous patterning of quantum dots at the air-water interface. Phys. Rev. E **1999**, 59, R6255.

(57) Isa, L.; Calzolari, D. C. E.; Pontoni, D.; Gillich, T.; Nelson, A.; Zirbs, R.; Sánchez-Ferrer, A.; Mezzenga, R.; Reimhult, E. Coreshell nanoparticle monolayers at planar liquid liquid interfaces: effects of polymer architecture on the interface microstructure. Soft Matter **2013**, 9, 3789–3797.

Graphical TOC Entry